This version of the article has been accepted for publication, after peer review and is subject to Springer Nature's AM terms of use, but ***is not the Version of Record and does not reflect post-acceptance improvements, or any corrections****. The Version of Record is available online at: https://doi.org/10.1038/s41561-022-00957-8 (full text: https://rdcu.be/cO4qr)*

Citation: Messié, M., Petrenko, A., Doglioli, A.M., Martinez, E., and Alvain, S. Basin-scale biogeochemical and ecological impacts of islands in the tropical Pacific Ocean. Nat. Geosci. 15, 469–474 (2022). https://doi.org/10.1038/s41561-022-00957-8

Basin-scale biogeochemical and ecological impacts of islands in the tropical Pacific Ocean

M. Messié[1,2,*], A. Petrenko[2], A. Doglioli[2], E. Martinez[3], and S. Alvain[4]

[1]Monterey Bay Aquarium Research Institute, Moss Landing, CA 95039, USA

[2]Aix Marseille Univ, Université de Toulon, CNRS, IRD, MIO, Marseille, France

[3]University of Brest, Ifremer, CNRS, IRD, Laboratoire d'Océanographie Physique et Spatiale (LOPS), IUEM, 29200 Brest, France

[4]Laboratoire d'Océanologie et de Géosciences, UMR 8187 – LOG, CNRS, Université de Lille, Université du Littoral Côte d'Opale, Wimereux, France

[*]corresponding author, monique@mbari.org

In the relatively unproductive waters of the tropical ocean, islands can enhance phytoplankton biomass and create hotspots of productivity and biodiversity that sustain upper trophic levels, including fish that are crucial to the survival of islands' inhabitants. This phenomenon, coined the "island mass effect" sixty-five years ago, has been widely described. However, most studies focused on individual islands, and very few documented phytoplankton community composition. Consequently, basin-scale impacts on phytoplankton biomass, primary production, and biodiversity remain largely unknown. Here we systematically identify enriched waters near islands from satellite chlorophyll concentration (a proxy for phytoplankton biomass) to analyze the island mass effect for all tropical Pacific islands on a climatological basis. We find enrichments near 99% of islands, impacting 3% of the tropical Pacific Ocean. We quantify local and basin-scale increases in chlorophyll and primary production by contrasting island-enriched waters with nearby waters. We also unveil, for the first time, a significant impact on phytoplankton community structure and biodiversity visible in anomalies in the ocean color signal. Our results suggest that, in addition to strong local biogeochemical impacts, islands may have even stronger and further reaching ecological impacts.

Phytoplankton, the tiny drifting algae that fix carbon dioxide via photosynthesis, are responsible for about half of the world's primary production[1] and support essentially all life in the open ocean. Their community composition and biodiversity have been tied to vertical carbon export, resource use efficiency, and ecological stability[2,3,4]. As such, phytoplankton biomass, production, and biodiversity have far-reaching impacts on marine ecosystems and the global carbon cycle. It is thus paramount to understand their environmental drivers so as to predict, and potentially mitigate, how they may change in the future. In most of the tropical ocean, nutrient supply is the

primary factor limiting phytoplankton growth[5]. Far from continents, nutrients are brought to the sunlit surface layer primarily by vertical mixing[6], wind- and eddy-driven upwelling[7], atmospheric deposition[8], nitrogen fixation[9], and horizontal advection[10]. Phytoplankton biodiversity is difficult to monitor; its patterns and drivers remain largely unknown even when focusing on the simplest of biodiversity metrics, richness (number of coexisting species). Several studies found high richness in warm, stable tropical regions and identified temperature as the primary phytoplankton richness driver[11,12]. Others described increased richness in dynamic regions[13], highlighting drivers such as nutrient supply rate and composition, advection, and top-down control[14].

Here, we focus on a phenomenon that has paradoxically received little attention at the basin scale, despite its prevalence and strong local impacts: island-driven increases in phytoplankton production, resulting in nearly ubiquitous chlorophyll enrichments near tropical Pacific islands and atolls[15]. This "island mass effect" (IME)[16] can result from various processes such as upwelling and mixing in lee eddies, island runoff, submarine groundwater discharge, and others (reviewed by Gove et al.[15]). These processes supply additional nutrients relative to surrounding waters, supporting enhanced phytoplankton growth and dramatically increasing local productivity. The resulting increased fish production is crucial to Pacific island societies that rely on fishing for food security and protein intake[17]. By increasing primary production, islands can also locally create an important oceanic sink for atmospheric CO_2 (as observed in the Southern Ocean[18]) and have been hypothesized to significantly contribute to the global carbon budget[19]. IMEs have been described for a few of the thousands of tropical Pacific islands, notably the Galapagos[20], Hawaii[21], the Marquesas[22], Kiribati[23], Solomon[24], New Caledonia[25], Tonga[26], Vanuatu, and Fiji[27]. There are also some rare reports of island impacts on phytoplankton community composition[28,29,30]. Only two studies systematically investigated the IME for several

islands at once: a compilation of *in situ* chlorophyll concentration in the south tropical Pacific[27], and an analysis of satellite chlorophyll increase near 35 coral reef islands and atolls[15]. Neither study considered phytoplankton community composition. A systematic study of the IME for all islands in the tropical Pacific, particularly addressing impacts on phytoplankton biodiversity, is unprecedented.

Characterizing island mass effects in the tropical Pacific

We investigated the IME for all tropical Pacific islands and shallow reefs using satellite surface chlorophyll concentrations (hereafter Chl). A total of 11,449 islands and 4,602 shallow reefs were identified from high-resolution coastline and bathymetry. Islands and reefs were combined within land pixels of the 4 km resolution Chl grid (pixels shallower than 30 m were treated as land, see Methods), resulting in a database of 437 islands and 227 shallow reefs (hereafter "islands"). An algorithm automatically detecting IMEs from Chl maps was developed and applied both to the time-averaged Chl and to a monthly climatology. For each island, the algorithm identified the IME as a Chl contour enclosing the island and surrounding high-Chl waters, termed IME region. A reference (REF) region of the same size was detected alongside each IME region, enclosing nearby non-IME waters (Extended Fig. 1). The REF region represents conditions that would exist if no IME was present. Increases in Chl nearby islands and within the IME regions were defined relative to REF.

The algorithm detected IMEs for most islands, whether in oligotrophic gyres or in more productive equatorial regions. Islands with the strongest, most far-reaching impacts on average Chl include the Marquesas, Fiji/Tonga, Solomon, Kiribati, and the Galapagos (Fig. 1). Most IMEs are strongly seasonal, such that an average map does not adequately render the IME

prevalence or strength. When applied to climatological maps (Fig. 1 inserts), the method detected an IME near 99% of islands (Table 1). Some of these IMEs only represent weak Chl increases because climatological averages smooth the IME signal, but their presence indicates that an IME likely occurred during the satellite time period. A more conservative approach still identified IMEs near 90% of islands (right column). If anything, the IME prevalence may be underestimated as small IMEs may not be detected using a 4-km resolution product (see Table S1). This confirms that the IME is nearly ubiquitous in the tropical Pacific[15]. Overall, our results indicate that the IME impacts 3% of the tropical Pacific area although islands and reefs together only represent 0.4%.

Island impacts on phytoplankton biomass and production

Local IME impacts were assessed by comparing the paired IME and REF regions, and total impacts calculated by summing the results over the entire tropical Pacific for each climatological month and averaging over time. The results reveal a strong impact of islands on surface phytoplankton biomass (using Chl as a proxy) and on satellite-derived primary production[31] (Table 1). Chl increases by 9% and primary production by 3% on average within IME regions. Next to the islands, impacts are even more dramatic with a Chl increase of 26% on average. The apparent higher impact on Chl than primary production is partially due to the lower spatial resolution of the primary production product (9 km vs 4 km for Chl), combined with the fact that pixels closest to islands, where impacts are greatest, must be removed (see Methods).

While local impacts are very high, islands seem to increase Chl and primary production by less than 1% over the tropical Pacific (Table 1). These numbers may be underestimated because of removing shallow pixels near islands where impacts are greatest, and because our algorithm

misses delayed IMEs occurring offshore[26] by assuming that the IME region is connected to the island. Although Chl measured by satellites is only representative of approximately a fifth of the euphotic zone, the relative impact on total vertically integrated phytoplankton biomass may be expected to be of the same order of magnitude as the impact on Chl since IME enrichments typically occur over the full euphotic zone[15].

The overall primary production increase around 0.05 PgC/yr (Table 1) can be compared to other processes, for which regional estimates of the nitrate supply carbon-equivalent (potential new production) are available. Potential new production represents an upper bound for new production, itself representing less than half of primary production in the region[32], which provides a basis for rough comparisons with the IME even though island-induced nutrient supply is unknown. These other processes include wind-driven upwelling (1.8 to 3.9 PgC/yr including equatorial upwelling when adapting past results to the region[33]), turbulent vertical mixing at the nitracline (0.4 PgC/yr for the region[6]), nitrogen fixation (around 0.2 PgC/yr for the Pacific[34], noting that nitrogen fixation may be partly supported by IMEs[28,26]), and the Peru upwelling system (0.1 PgC/yr[35]). Consequently, despite strong local impacts, islands are unlikely to represent a major source of nutrients for phytoplankton in the tropical Pacific and to play an important role in the global carbon budget.

Island impacts on phytoplankton taxonomy

Assessing island impacts on phytoplankton species composition is a challenging proposition. There is at present no *in situ* dataset with the taxonomic and spatiotemporal coverage needed to describe phytoplankton community structure and biodiversity throughout the tropical Pacific. Significant progress has been made towards identifying phytoplankton taxonomy from space[36],

but published methods only identify a small number of broad taxonomic groups or size classes. To circumvent the lack of taxonomic resolution in satellite products, we used PHYSAT[37], a method clustering anomalies in the ocean color signal into 61 phenological bio-optical classes[38] (hereafter phenoclasses, see Methods). Because phytoplankton characteristics such as cell size, composition, intracellular structure, cell arrangement, and absorption impact the ocean color signal, phenoclasses are representative of various phytoplankton communities[39]. We applied classical ecological metrics to phenoclasses, capturing changes in phenoclass composition and diversity between IME and REF regions. These ecological metrics describe island-driven changes in phenoclasses, themselves revealing changes in phytoplankton taxonomy.

Island impacts on phytoplankton community composition were studied using the Bray-Curtis dissimilarity index applied to phenoclasses (Fig. 2a). High phenoclass dissimilarity was identified between IME and REF regions for most islands, particularly at low latitudes, suggesting a strong island impact on phytoplankton community composition. These differences are considerably higher than between random sets of pixels encompassing the IME and REF regions (Fig. 3a left), confirming that they are significant and not due to random spatial heterogeneity in PHYSAT phenoclasses. We looked more closely at the most common phenoclasses found in the tropical Pacific. These are part of "labeled" phenoclasses that were matched to dominant broad taxonomic groups thanks to coincident in situ data. The corresponding phytoplankton groups are mostly *Prochlorococcus*, followed by nanoplankton and *Synechococcus*, consistent with known phytoplankton composition in the region[40]. *Prochlorococcus*-labeled phenoclasses significantly decreased in proportion within the IME region relative to REF, while *Synechococcus*- and nanoplankton-labeled phenoclasses both

increased, albeit non-significantly for nanoplankton (Fig. 3a right). This is coherent with reports of *Synechococcus* and nanoplankton outcompeting *Prochlorococcus* at higher nutrient levels[41,42].

Island impacts on phytoplankton biodiversity were investigated using several dimensions of phenoclass diversity: richness (number of distinct phenoclasses), evenness (phenoclass proportion homogeneity), and the Shannon index, a widely used biodiversity metric that accounts for both richness and evenness (Table 1). On average, phenoclass richness strongly increases near islands, more than Chl and primary production. The island-driven phenoclass richness increase is spatially variable (Fig. 2b), highest poleward of 10° latitude in both hemispheres. There is no impact on evenness, and a smaller impact on Shannon diversity. Part of the richness increase simply arises because, by definition, Chl is higher in IME than REF regions (Fig. 3b, left). Indeed, phenoclass richness is strongly correlated with Chl ($r = 0.72$ across REF regions, Extended Fig. 3), consistent with *in situ* phytoplankton richness patterns in low productivity waters[43]. However, the island-driven increase in phenoclass richness is only weakly correlated to the Chl increase ($r = 0.22$), suggesting that this Chl signal only explains part of the phenoclass richness increase. We randomly selected two thirds of the IME and REF regions with similar Chl characteristics, effectively removing the Chl signal (Extended Fig. 4). A total of 1,000 random permutations were selected, and 33% of permutations still displayed significantly higher phenoclass richness within the IME subset (Fig. 3b, right). Taken together, these results suggest that the observed island-driven increase in phenoclass richness is not only linked to increased Chl, but also partly due to some island-specific phenomenon. We hypothesize that some islands release nutrients with ratios different from the ones of ambient waters, depending on soil composition and human activities, which could favor different species and increase phytoplankton richness[14]. By contrast, weaker taxonomic impacts would be expected near

seamounts[44], because seamount-driven enrichments result from upwelling and mixing[45] of water masses close to Redfield ratios.

Our satellite-based findings provide compelling evidence for a strong IME impact on phytoplankton community composition and biodiversity. While PHYSAT is only a proxy for phytoplankton taxonomy, our results match previous reports from the Marquesas islands, including a shift from *Prochlorococcus* to *Synechococcus* and an increase in phytoplankton biodiversity leeward of the islands[29,30]. This island-driven increase in phytoplankton biodiversity may be a crucial piece contributing to islands being biodiversity hotspots in the world oceans[46]. Island effects could also contribute to the observed latitudinal maximum phytoplankton richness in the tropics[11,12], since islands can export biodiversity to surrounding waters[46]. Observations of phytoplankton taxonomy around other islands are needed to confirm PHYSAT-inferred island impacts on phytoplankton community composition and biodiversity.

Regardless of impacts on phytoplankton taxonomy, local impacts on biomass and productivity are so high that regions enriched by IMEs represent oases in an otherwise largely unproductive environment (Fig. 1). There is strong evidence that they attract fish and marine predators[47,48], and represent important stopovers along marine migration corridors[49]. While fishery data would be biased for islands (due to confounding effects of higher fish biomass and proximity), a recent study of seamounts found a more than doubled fish catch at seamounts with Chl enhancements relative to seamounts without[45]. Some islands such as Hawaii and the Galapagos also represent key conservation sites deemed irreplaceable because of the presence of endemic marine species[50]. This suggests that islands have profound ecological consequences both at the local and basin scale, even though large-scale impacts on primary production appear to be small.

Acknowledgements

M.M. was funded by the European Union's Horizon 2020 research and innovation programme under the Marie Skłodowska-Curie grant agreement SAPPHIRE No. 746530, and by the David and Lucile Packard Foundation. The project leading to this publication has received funding from European FEDER Fund under project 1166-39417 (M.M., A.P., A.D.). We thank Anne-Hélène Rêve-Lamarche and David Dessailly for their help extracting and using the PHYSAT outputs, and Eric Pape for useful comments and text edits. The box plots in Fig. 3 were generated using the IoSR Matlab toolbox (https://github.com/IoSR-Surrey/MatlabToolbox), and maps displayed using m_map (https://www.eoas.ubc.ca/~rich/map.html).

Author Contributions Statement

M.M. conceived and designed the study, with input from A.P., A.D., and S.A. M.M. developed the IME algorithm with input from A.P. and A.D., performed the data analyses, and led the interpretations and writing. S.A. provided the PHYSAT outputs. A.P., A.D., E.M., and S.A. provided significant input on the text, and contributed to discussions that shaped the study and the manuscript.

Competing Interests Statement

The authors declare no competing interests.

Tables

	All IMEs	IMEs with Chl increase nearby islands ≥ 10%
IME prevalence		
Percentage of islands with IME detected at least one month a year	98.9%	90.1%
… at least 6 months a year	93.2%	55.1%
… year-long	44.3%	23.9%
Percentage of IME detections over all possible cases (664 islands, 12 months)	83.7%	54.2%
IME spatial impact		
Average IME area	8,001 km²	13,558 km²
Total IME area within the tropical Pacific (in percentage)	3,179,873 km² (3.2%)	3,033,672 km² (3.1%)
IME impact on surface chlorophyll concentration (Chl)		
Average nearby percentage Chl increase (pixels closest to island)	25.6%	40.8%
Average percentage Chl increase per IME	9.3%	13.1%
Average total Chl increase per IME (summed over the IME area)	0.21 tons/m	0.37 tons/m
Total IME-induced Chl increase in the tropical Pacific (in percentage)	83 tons/m (0.68%)	82 tons/m (0.67%)
IME impact on primary production (PP)		
Average percentage PP increase per IME	2.8%	4.2%
Average total PP increase per IME (summed over the IME area)	0.14 TgC/yr	0.23 TgC/yr
Total IME-induced PP increase in the tropical Pacific (in percentage)	50.4 TgC/yr (0.51%)	50.2 TgC/yr (0.51%)
IME impact on PHYSAT phenoclass diversity		
Average percentage richness increase per IME	12.1%	13.2%
Average percentage evenness increase per IME	-0.1%	0.0%
Average percentage Shannon index increase per IME	4.1%	4.5%

Table 1: IME impacts in the tropical Pacific. IME prevalence is defined based on islands belonging to an IME region (there can be several islands associated with one IME region). "Average" impact refers to impact for a single IME, averaged over all detected IMEs. They include both change in ambient conditions in IME vs REF regions, and total island-driven increase summed over the IME area. "Total" impact refers to impacts summed over the entire study region and averaged over a climatological year. Phenoclass diversity impacts were computed for IME/REF regions of at least 100 PHYSAT data points, and richness was

normalized to 100 data points to correct for the strong dependence of richness on area sampled (see Methods). Statistics are given for all IMEs, and for a more conservative subset excluding those where the island nearby Chl increase was below 10%. Additional metrics (median and interquartile range) are provided in Extended Table 1.

Figure legends

Figure 1: Map of IME detection in the tropical Pacific. The main map represents the 2002-2018 average satellite chlorophyll concentration (MODIS data) in the study region (30°S - 30°N). IME regions are contoured in different shades of red depending on Chl increase nearby islands relative to a reference region (maximum value in mean conditions: 558% observed for the Galapagos Islands). Inserts display the climatological month with the highest IME chlorophyll enrichment in selected regions with a custom color bar: A- Kiribati in May, B- Hawaii in September, C- Galapagos in January, D- Solomon in July, E- New Caledonia, Vanuatu, Fiji, and Tonga in February, and F- Marquesas in May. Extended Fig. 2 provides full maps of climatological months.

Figure 2: Maps of island impacts on PHYSAT phenoclasses, indicative of impacts on phytoplankton community composition and biodiversity. For each island, the maximum value observed over the seasonal cycle is displayed (only computed for IME regions containing at least 100 PHYSAT data points). a) Phenoclass Bray-Curtis dissimilarity between IME and REF regions, indicative of differences in phenoclass composition. b) Phenoclass richness increases in the IME region relative to REF (richness was normalized to 100 data points). c) Summary of island impacts on phenoclasses, defined according to the median value for phenoclass Bray-Curtis dissimilarity (composition, pink) and for richness increase (richness, blue), where "impacts" are defined as above the median. Phenoclass richness increase is correlated with absolute latitude ($r = 0.18$) while phenoclass Bray-Curtis dissimilarity is anticorrelated ($r = -0.24$). Despite their opposite relation to latitude, phenoclass richness increase and Bray-Curtis dissimilarity are actually weakly correlated ($r = 0.30$).

Figure 3: Island impacts on phytoplankton community structure as depicted by PHYSAT. Statistics are based on paired climatological IME/REF regions with 100 PHYSAT data points minimum. Box plots report the median (center line), 95% confidence interval around the median (notches equal to ±1.58 times interquartile range divided by square root of the sample size), interquartile range (box), and 1.5 times the interquartile range (whiskers). Data points are displayed as crosses (outliers beyond whiskers as dots). Symbols show whether distributions are statistically different according to a Mann-Whitney U-test (= is non-significant, +/- indicate how IME medians relate to REF).

a) Left: Phenoclass Bray-Curtis dissimilarity between IME and REF regions, compared to data points randomly taken across IME/REF regions. Right: Occurrence frequency of dominant phenoclasses (frequency >0.02) in the IME and REF regions, sorted by label: *Prochlorococcus* (Pros), *Synechococcus* (Syn), and nanoplankton (Nano).

b) Left 2 panels: Phenoclass richness is significantly higher in IME than in REF regions (9.6% difference in median) partly linked to higher Chl (12.4% difference in median). Right: summary of Chl and phenoclass richness characteristics for 1000 random permutations independently taken within IME and REF regions (N=712) such that their Chl distribution is equivalent ($p>0.05$). Chl may be insignificantly higher within IME or REF subsets (as described by the difference in median) because IME/REF pairs are decoupled (example in Extended Fig. 4).

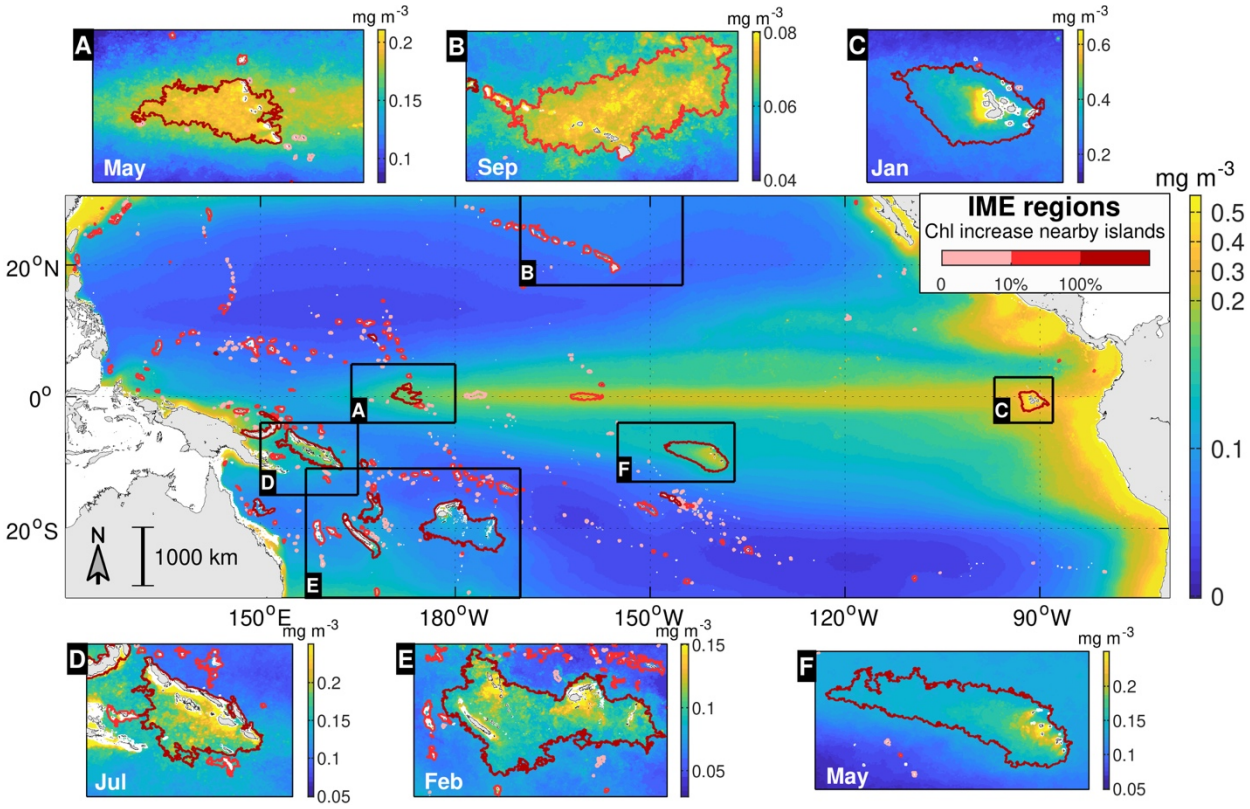

A
May
mg m-3
0.2
0.15
0.1
B
Sep
mg m-3
0.08
0.06
0.04
C
Jan
mg m-3
0.6
0.4
0.2
mg m-3
0.5
0.4
0.3
0.2
0.1
0
IME regions
Chl increase nearby islands
0
10%
100%
20°N
0°
20°S
N
1000 km
150°E
180°W
150°W
120°W
90°W
D
Jul
mg m-3
0.2
0.15
0.1
0.05
E
Feb
mg m-3
0.15
0.1
0.05
F
May
mg m-3
0.2
0.15
0.1
0.05

Figure 1.

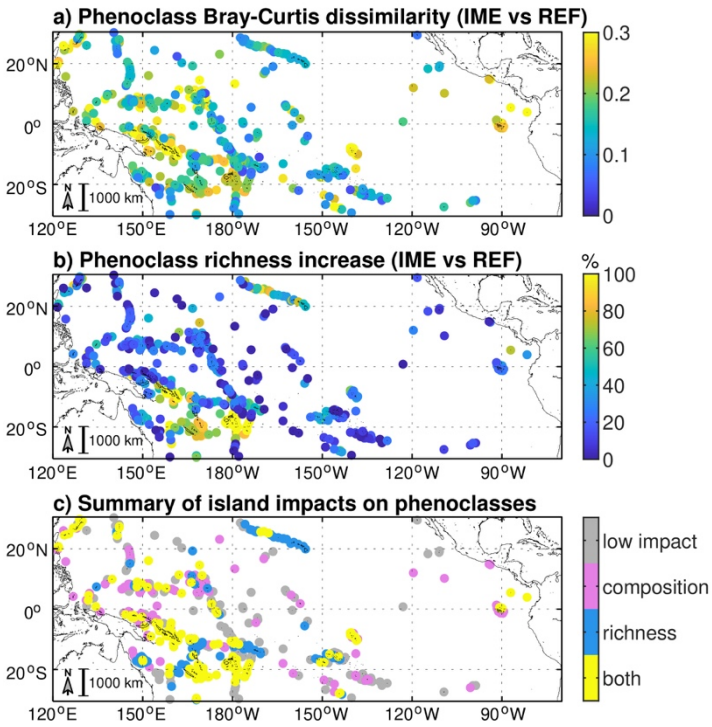

a) Phenoclass Bray-Curtis dissimilarity (IME vs REF)
0.3
0.2
0.1
0
b) Phenoclass richness increase (IME vs REF)
%
100
80
60
40
20
0
c) Summary of island impacts on phenoclasses
low impact
composition
richness
both
20°N
0°
20°S
1000 km
120°E
150°E
180°W
150°W
120°W
90°W

Figure 2.

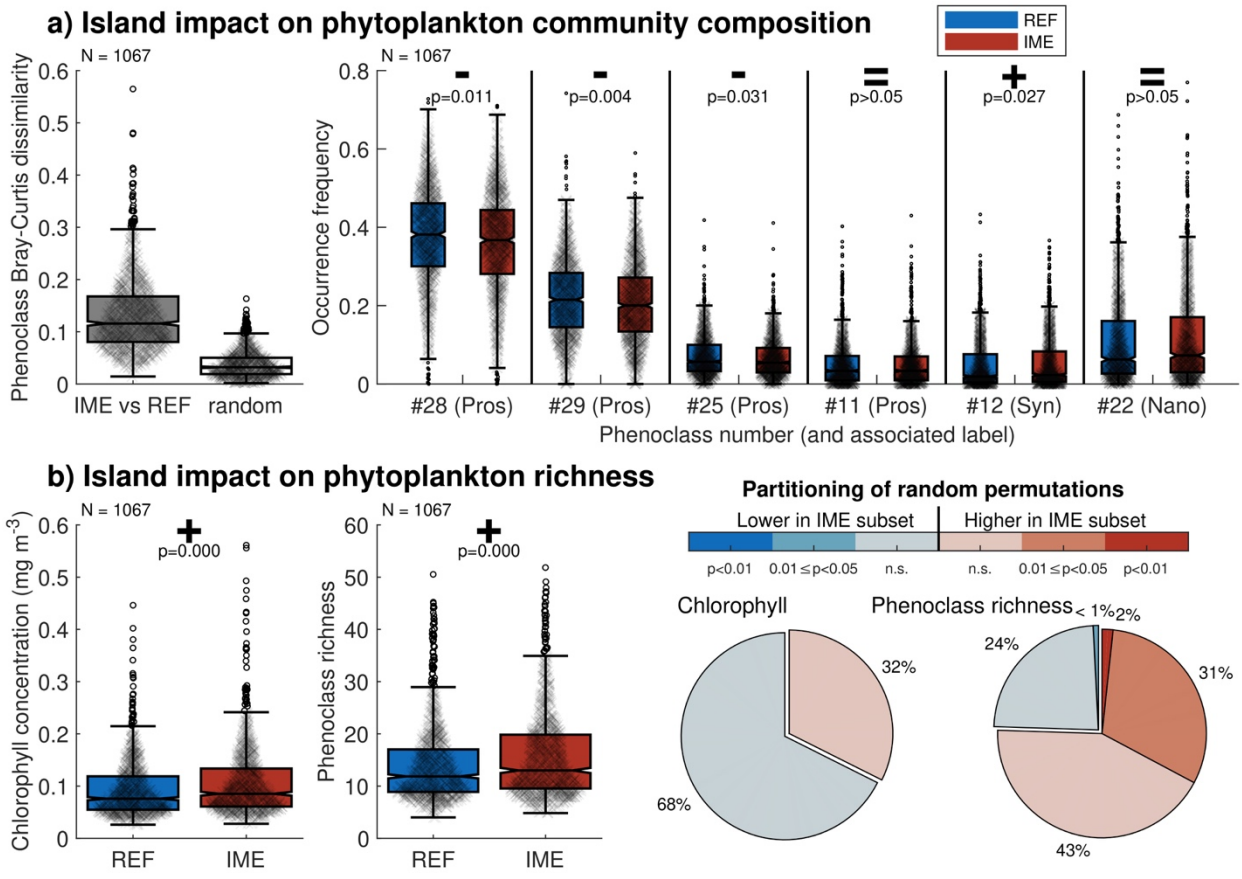

a) Island impact on phytoplankton community composition
REF
IME
N = 1067
Phenoclass Bray-Curtis dissimilarity
IME vs REF
random
N = 1067
Occurrence frequency
p=0.011
*p=0.004
p=0.031
p>0.05
p=0.027
p>0.05
#28 (Pros)
#29 (Pros)
#25 (Pros)
#11 (Pros)
#12 (Syn)
#22 (Nano)
Phenoclass number (and associated label)
b) Island impact on phytoplankton richness
N = 1067
Chlorophyll concentration (mg m-3)
p=0.000
REF
IME
N = 1067
Phenoclass richness
p=0.000
REF
IME
Partitioning of random permutations
Lower in IME subset
Higher in IME subset
p<0.01
0.01≤p<0.05
n.s.
n.s.
0.01≤p<0.05
p<0.01
Chlorophyll
32%
68%
Phenoclass richness
< 1%
2%
24%
31%
43%

Figure 3.

References

1. Field, C. B., M. J. Behrenfeld, J. T. Randerson & P. Falkowski (1998), Primary production of the biosphere: integrating terrestrial and oceanic components, Science, 281(5374), 237-240, https://doi.org/10.1126/science.281.5374.237

2. Guidi, L., S. Chaffron, L.,Bittner, D. Eveillard, A. Larhlimi, S. Roux et al. (2016), Plankton networks driving carbon export in the oligotrophic ocean, Nature, 532(7600), 465-470, https://doi.org/10.1038/nature16942

3. Ptacnik, R., A. G. Solimini, T. Andersen, T. Tamminen, P. Brettum, L. Lepistö, E. Willén & S. Rekolainen (2008), Diversity predicts stability and resource use efficiency in natural phytoplankton communities, Proc. Natl. Acad. Sci., 105(13), 5134-5138, https://doi.org/10.1073/pnas.0708328105

4. Corcoran, A. A. & W. J. Boeing (2012), Biodiversity increases the productivity and stability of phytoplankton communities, PLoS ONE, 7(11), e49397, https://doi.org/10.1371/journal.pone.0049397

5. Arteaga, L., M. Pahlow & A. Oschlies (2014), Global patterns of phytoplankton nutrient and light colimitation inferred from an optimality-based model, Global Biogeochem. Cycles, 28(7), 648-661, https://doi.org/10.1002/2013GB004668

6. Lewis, M., D. Hebert, W. G. Harrison, T. Platt & N. S. Oakey (1986), Vertical nitrate fluxes in the oligotrophic ocean, Science, 234(4778), 870-873, https://doi.org/10.1126/science.234.4778.870

7. McGillicuddy, D. J. J., A. A. Laurence, N. R. Bates, T. Bibby, K. O. Buesseler, C. A. Carlson et al. (2007), Eddy/wind interactions stimulate extraordinary mid-ocean plankton blooms, Science, 316(5827), 1021-1026, https://doi.org/10.1126/science.1136256

8. Duce, R. A., J. LaRoche, K. Altieri, K. R. Arrigo, A. R. Baker, D. G. Capone et al. (2008), Impacts of atmospheric anthropogenic nitrogen on the open ocean, Science, 320(5878), 893-897, https://doi.org/10.1126/science.1150369

9. Tang, W., S. Wang, D. Fonseca-Batista, F. Dehairs, S. Gifford, A. G. Gonzalez et al. (2019), Revisiting the distribution of oceanic N2 fixation and estimating diazotrophic contribution to marine production, Nat. Commun., 10(1), https://doi.org/10.1038/s41467-019-08640-0

10. Letscher, R. T., F. Primeau & J. K. Moore (2016), Nutrient budgets in the subtropical ocean gyres dominated by lateral transport, Nat. Geosci., 9(11), 815-819, https://doi.org/10.1038/ngeo2812

11. Righetti, D., M. Vogt, N. Gruber, A. Psomas & N. E. Zimmermann (2019), Global pattern of phytoplankton diversity driven by temperature and environmental variability, Sci. Adv., 5(5), eaau6253, https://doi.org/10.1126/sciadv.aau6253

12. Ibarbalz, F. M., Henry, N., Brandão, M. C., Martini, S., Busseni, G., Byrne, H. et al. (2019), Global trends in marine plankton diversity across kingdoms of life, Cell, 179(5), 1084-1097.e21, https://doi.org/10.1016/j.cell.2019.10.008

13. Lévy, M., P. J. S. Franks & K. S. Smith (2018), The role of submesoscale currents in structuring marine ecosystems, Nat. Commun., 9(1), https://doi.org/10.1038/s41467-018-07059-3

14. Dutkiewicz, S., P. Cermeno, O. Jahn, M. J. Follows, A. E. Hickman, D. A. A. Taniguchi & B. A. Ward (2020), Dimensions of marine phytoplankton diversity, Biogeosciences, 17(3), 609-634, https://doi.org/10.5194/bg-17-609-2020

15. Gove, J. M., M. A. McManus, A. B. Neuheimer, J. J. Polovina, J. C. Drazen, C. R. Smith et al. (2016), Near-island biological hotspots in barren ocean basins, Nat. Commun., 7, 10581, https://doi.org/10.1038/ncomms10581

16. Doty, M. S. & M. Oguri (1956), The island mass effect, J. Cons. Int. Explor. Mer., 22(1), 33-37, https://doi.org/10.1093/icesjms/22.1.33

17. Bell, J. D., M. Kronen, A. Vunisea, W. J. Nash, G. Keeble, A. Demmke, S. Pontifex & S. Andréfouët (2009), Planning the use of fish for food security in the Pacific, Marine Policy, 33(1), 64-76, https://doi.org/10.1016/j.marpol.2008.04.002

18. Bakker, D. C., M. C. Nielsdóttir, P. J. Morris, H. J. Venables & A. J. Watson (2007), The island mass effect and biological carbon uptake for the subantarctic Crozet Archipelago, Deep Sea Research Part II: Topical Studies in Oceanography, 54(18-20), 2174-2190, https://doi.org/10.1016/j.dsr2.2007.06.009

19. Heywood, K. J., D. P. Stevens & G. R. Bigg (1996), Eddy formation behind the tropical island of Aldabra, Deep Sea Res. Part I, 43(4), 555-578, https://doi.org/10.1016/0967-0637(96)00097-0

20. Palacios, D. M. (2002), Factors influencing the island-mass effect of the Galapagos archipelago, Geophys. Res. Lett., 29(23), 2134, https://doi.org/10.1029/2002GL016232

21. Gilmartin, M. & N. Revelante (1974), The 'island mass' effect on the phytoplankton and primary production of the Hawaiian Islands, J. Exp. Mar. Biol. Ecol., 16(2), 181-204, https://doi.org/10.1016/0022-0981(74)90019-7

22. Signorini, S. C., C. R. McClain & Y. Dandonneau (1999), Mixing and phytoplankton bloom in the wake of the Marquesas Islands, Geophys. Res. Lett., 26(20), 3121-3124, https://doi.org/10.1029/1999GL010470

23. Messié, M., M.-H. Radenac, J. Lefèvre & P. Marchesiello (2006), Chlorophyll bloom in the western Pacific at the end of the 1997-98 El Niño: the role of the Kiribati Islands, Geophys. Res. Lett., 33, L14601, https://doi.org/10.1029/2006GL026033

24. Messié, M. & M.-H. Radenac (2006), Seasonal variability of the surface chlorophyll in the western tropical Pacific from SeaWiFS data, Deep Sea Res. Part I, 53(10), 1581-1600, https://doi.org/10.1016/j.dsr.2006.06.007

25. Le Borgne, R., Y. Dandonneau & L. Lemasson (1985), The problem of the island mass effect on chlorophyll and zooplankton standing crops around Mare (Loyalty Islands) and New Caledonia, Bull. Mar. Sci., 37(2), 450-459

26. Messié, M., A. Petrenko, A. M. Doglioli, C. Aldebert, E. Martinez, G. Koenig, S. Bonnet & T. Moutin (2020), The delayed island mass effect: How islands can remotely trigger blooms in the oligotrophic ocean, Geophys. Res. Lett., 47(2), https://doi.org/10.1029/2019gl085282

27. Dandonneau, Y. & L. Charpy (1985), An empirical approach to the island mass effect in the south tropical Pacific based on sea surface chlorophyll concentrations, Deep Sea Research Part A, 32, 707-721, https://doi.org/10.1016/0198-0149(85)90074-3

28. Shiozaki, T., T. Kodama & K. Furuya (2014), Large-scale impact of the island mass effect through nitrogen fixation in the western South Pacific Ocean, Geophys. Res. Lett., 41(8), 2907-2913, https://doi.org/10.1002/2014GL059835

29. Caputi, L., Q., Carradec, D., Eveillard, A., Kirilovsky, E., Pelletier, J. J. P. Karlusich et al. (2019), Community-level responses to iron availability in open ocean plankton ecosystems, Global Biogeochem. Cycles, 33(3), 391-419, https://doi.org/10.1029/2018gb006022

30. Martinez, E., M. Rodier, M. Pagano & R. Sauzède (2020), Plankton spatial variability within the Marquesas archipelago, South Pacific, J. Mar. Syst., 212, 103432, https://doi.org/10.1016/j.jmarsys.2020.103432

31. Behrenfeld, M. J. & P. G. Falkowski (1997), Photosynthetic rates derived from satellite-based chlorophyll concentration, Limnol. Oceanogr., 42(1), 1-20, https://doi.org/10.4319/lo.1997.42.1.0001

32. Laws, E. A., H. Ducklow & J. J. McCarthy (2000), Temperature effects on export production in the open ocean, *Global Biogeochem. Cycles*, *14*(4), 1231-1246, https://doi.org/10.1029/1999GB001229

33. Messié, M. & F. P. Chavez (2012), A global analysis of ENSO synchrony: the oceans' biological response to physical forcing, J. Geophys. Res., 117, C09001, https://doi.org/10.1029/2012JC007938

34. Luo, Y.-W., I. D. Lima, D. M. Karl, C. A. Deutsch & S. C. Doney (2014), Data-based assessment of environmental controls on global marine nitrogen fixation, Biogeosciences, 11(3), 691-708, https://doi.org/10.5194/bg-11-691-2014

35. Messié, M. & F. P. Chavez (2015), Seasonal regulation of primary production in eastern boundary upwelling systems, Prog. Oceanogr., 134, 1-18, https://doi.org/10.1016/j.pocean.2014.10.011

36. Mouw, C. B., N. J. Hardman-Mountford, S. Alvain, A. Bracher, R. J. W. Brewin, A. Bricaud et al. (2017), A Consumer's guide to satellite remote sensing of multiple phytoplankton groups in the global ocean, Front. Mar. Sci., 4, 41, https://doi.org/10.3389/fmars.2017.00041

37. Alvain, S., C. Moulin, Y. Dandonneau & F. M. Bréon (2005), Remote sensing of phytoplankton groups in case 1 waters from global SeaWiFS imagery, Deep Sea Res. Part I, 52(11), 1989-2004, https://doi.org/10.1016/j.dsr.2005.06.015

38. Rêve-Lamarche, A.-H., S. Alvain, M.-F. Racault, D. Dessailly, N. Guiselin, C. Jamet, V. Vantrepotte & G. Beaugrand (2017), Ocean Color Radiance Anomalies in the North Sea, Front. Mar. Sci., https://doi.org/10.3389/fmars.2017.00408

39. Alvain, S., H. Loisel & D. Dessailly (2012), Theoretical analysis of ocean color radiances anomalies and implications for phytoplankton groups detection in case 1 waters, Opt. Express, 20(2), 1070, https://doi.org/10.1364/oe.20.001070

40. Mackey, D. J., J. Blanchot, H. W. Higgins & J. Neveux (2002), Phytoplankton abundances and community structure in the equatorial Pacific, Deep Sea Res. Part II, 49(13-14), 2561-2582, https://doi.org/10.1016/S0967-0645(02)00048-6

41. Johnson, Z. I. (2006), Niche partitioning among Prochlorococcus ecotypes along ocean-scale environmental gradients, Science, 311(5768), 1737-1740, https://doi.org/10.1126/science.1118052

42. Martiny, A. C., S. Kathuria & P. M. Berube (2009), Widespread metabolic potential for nitrite and nitrate assimilation among Prochlorococcus ecotypes, Proc. Natl. Acad. Sci., 106(26), 10787-10792, https://doi.org/10.1073/pnas.0902532106

43. Vallina, S. M., M. J. Follows, S. Dutkiewicz, J. M. Montoya, P. Cermeno & M. Loreau (2014), Global relationship between phytoplankton diversity and productivity in the ocean, Nat. Commun., 5(1), https://doi.org/10.1038/ncomms5299

44. Dai, S., Y. Zhao, X. Li, Z. Wang, M. Zhu, J. Liang, et al. (2020), The seamount effect on phytoplankton in the tropical western Pacific, Mar. Environ. Res., 105094, https://doi.org/10.1016/j.marenvres.2020.105094

45. Leitner, A. B., A. B. Neuheimer & J. C. Drazen (2020), Evidence for long-term seamount-induced chlorophyll enhancements, Sci. Rep., 10(1), https://doi.org/10.1038/s41598-020-69564-0

46. Bowen, B. W., L. A. Rocha, R. J. Toonen & S. A. Karl (2013), The origins of tropical marine biodiversity, Trends in Ecology & Evolution, 28(6), 359-366, https://doi.org/10.1016/j.tree.2013.01.018

47. Worm, B., H. K. Lotze & R. A. Myers (2003), Predator diversity hotspots in the blue ocean, Proc. Natl. Acad. Sci., 100(17), 9884-9888, https://doi.org/10.1073/pnas.1333941100

48. Block, B. A., I. D., Jonsen, S. J., Jorgensen, S. A., Winship, S. A., Shaffer, S. J. Bograd et al. (2011), Tracking apex marine predator movements in a dynamic ocean, Nature, 475, 86-90, https://doi.org/10.1038/nature10082

425 49. Harrison, A.-L., D. P. Costa, A. J. Winship, S. R. Benson, S. J. Bograd, M. Antolos et al.
426 (2018), The political biogeography of migratory marine predators, Nature Ecology &
427 Evolution, 2(10), 1571-1578, https://doi.org/10.1038/s41559-018-0646-8
428 50. Pompa, S., P. R. Ehrlich & G. Ceballos (2011), Global distribution and conservation of
429 marine mammals, Proc. Natl. Acad. Sci., 108(33), 13600-13605,
430 https://doi.org/10.1073/pnas.1101525108
431

Methods

IME detection data sets. The IME was detected from a climatology of MODIS satellite surface chlorophyll-*a* concentrations (Chl, 4 km, monthly from July 2002 to December 2018, erdMH1chlamday product downloaded from https://coastwatch.pfeg.noaa.gov/erddap/info/index.html). The study was based on the 4 km MODIS Chl grid in the tropical Pacific (30°N/30°S; east/west borders are roughly delimited by the Americas, Australia, Indonesia, Philippines, and Taiwan, see Fig. 1). Islands were detected from the Global Self-consistent, Hierarchical, High-resolution Geography Database (GSHHG) version 2.3.7 full resolution coastline (https://www.ngdc.noaa.gov/mgg/shorelines/gshhs.html) loaded using functions from the m_map toolbox (https://www.eoas.ubc.ca/~rich/map.html). Bathymetry was obtained from the GEBCO global bathymetry (https://www.gebco.net/data_and_products/gridded_bathymetry_data/) at 1/15' resolution (< 500 m). A 4 km resolution "shallow mask" was generated for the MODIS grid, including all pixels containing land shallower than 30 m according to GEBCO or where an island was detected. The shallow mask was extended by one additional pixel in all directions to ensure that all pixels containing shallow waters were flagged[15]. All ocean color data (Chl, primary production, and PHYSAT, see below) were removed within the shallow mask as they were potentially contaminated by bottom reflectance[15]. In practice, pixels within the shallow mask (containing land, waters shallower than 30 m, and adjacent pixels) were treated as land.

Island database. The island database includes both emerged islands and reefs shallower than 30 m according to the GEBCO bathymetry. The reason is that some atolls can have no consistent (e.g., tide-dependent) or very little emerged land, and can potentially be missed both by GSHHG and by the GEBCO bathymetry. Islands and reefs were identified as follows. Islands were

455 detected from the GSHHS coastline as closed contours in the 120°E-70°W, 30°S-30°N region.
456 Because GSHHG was constructed from databases that were built in the 70s and 80s, errors
457 remained in the location of some islands. Islands being too numerous to all be validated, only
458 islands from the final database (see below) were checked against GEBCO bathymetry, and where
459 obvious discrepancies existed, their position was shifted accordingly. The island database was
460 then reprocessed until no more discrepancy was found (total corrected islands: n=32). The island
461 database was merged with a published database of 1,779 islands[51] by finding, for each island
462 from the Nunn et al. database[51], the closest GSHHS contour. The Nunn et al. database[51] provides
463 more precise information regarding position, elevation, island type, and area. Last, reefs were
464 detected from GEBCO (at < 500 m resolution) as groups of pixels shallower than 30 m ("shallow
465 zones", n=5,972), that include both submerged reefs and emerged islands. Island and reef
466 databases were merged by finding islands within shallow zones, when they existed. The
467 combined dataset after removing contours within the east/west mask (e.g., Atlantic, Indonesia)
468 includes 16,051 islands and reefs (hereafter "islands"). Islands within 100 km of the tropical
469 Pacific east/west borders were removed to avoid continental influences (n=5,062). The remaining
470 islands were then combined within the MODIS shallow mask (see section above and Fig. S1).
471 The term "island" in the paper thus refers to a group of islands/reefs belonging to a set of
472 connected shallow pixels. The final database includes 664 islands (437 with emerged lands,
473 including 363 from the Nunn et al. island database[51], and 227 shallow reefs).

474 **IME detection.** The IME was defined for each island as the smallest possible Chl contour
475 enclosing the island that fulfills a list of criteria detailed below (see Fig. S2 for a representation
476 of the algorithm). Beforehand, the maximum (Chl_max) and minimum (Chl_min) nearby Chl
477 were obtained for each island within a 1-pixel band around the island mask. Islands were ranked

by Chl_min, and processed from lowest to highest Chl_min. For a given island, the IME Chl contour (termed cChl) was iteratively lowered by 0.01 mg m^{-3} starting at Chl_max and the corresponding IME mask computed. The IME mask includes both pixels above cChl and adjacent missing data, such that other islands can become part of the same IME, then termed "shared IME". When this happened, Chl_max was adjusted to the highest value; Chl_min does not need adjustment since islands are processed in Chl_min order. The iteration was stopped when one of the following conditions was met: (1) cChl < Chl_min (the rationale being that currents displace the nutrient enrichment downstream of the island, so that at least one pixel surrounding the island should not belong to the IME); (2) the IME mask was too large, either touching the domain borders, or touching the continent masks or adjacent NaN pixels (this happens when contours enclose the full oligotrophic gyre); (3) regions of high Chl (> 0.8*Chl_max) were found within the IME mask, further than 32 pixels away from any island (~ 150 km). In this last case, the goal was to avoid non-island sources of nutrients within the IME region such as open-ocean eddies or upwelling; the 32-pixel tolerance deals with cases where the Chl maximum is displaced downstream of the islands[52]. The IME peak can occur even further downstream, notably in cases of delayed IME[26]; 32 pixels thus represents a compromise between capturing most IMEs and avoiding non-IME local Chl enrichments. While sensitive to the parameters used, this criterium only concerned 1.3% of cases (for the monthly climatology); in 95% of cases, the algorithm stops due to criterion #2. When one of the 3 criteria was met, a second iteration was performed at higher resolution (0.001 mg m^{-3}) starting with the last cChl until meeting the criteria again, such that cChl was determined with a 0.001 mg m^{-3} accuracy. This is well beyond measured Chl accuracy, but small changes in cChl can result in large changes in IME areas on climatological averages, hence the need for high sensitivity. The IME

was only kept if the IME mask contained at least 2 Chl pixels. The IME detection algorithm is available at https://bitbucket.org/messiem/toolbox_IME_detection.

Satellite-derived information on phytoplankton biomass and primary production. Island impacts were assessed using satellite chlorophyll-*a* (Chl), a common proxy for phytoplankton biomass[53] representative of the top ~ 10-30 m in our region (first optical depth). Subsurface impacts remain unknown; in some cases, apparent surface enrichments can result from the passive uplift of the deep chlorophyll maximum without any net biomass increase[54]. However, in situ profiles available near islands suggest this is the exception rather than the rule[15] (see also Table S3). Island impacts on primary production were estimated using the MODIS-based standard Vertically Generalized Production Model[31] (VGPM). The VGPM estimates primary production integrated over the euphotic depth range based on satellite chlorophyll, light availability, and temperature (a proxy for nutrient availability), and has been widely used for large-scale studies for which the spatiotemporal coverage of in situ data remains insufficient. Results are similar when using a more recent primary production algorithm (CAFE model[55]): total IME-induced PP increase = 44.9 TgC/yr vs 50.4 TgC/yr for the VGPM (Table 1). Primary production was downloaded from the Ocean Productivity website (http://science.oregonstate.edu/ocean.productivity/index.php) at 9 km resolution for the period July 2002 - December 2018 (see above for Chl data information). Primary production maps were averaged into a monthly climatology, pixels shallower than 30 m removed, and data interpolated on the Chl grid (4 km resolution). The lower resolution of the primary production product means that areas larger than for Chl were impacted by the shallow pixel removal, effectively removing high values near islands more than for Chl; the corresponding pixels on the Chl grid (i.e. outside of the Chl shallow mask) were interpolated using a median filter.

Island-driven impacts on chlorophyll and primary production. Island impacts were assessed by contrasting data in the IME region to data in a reference region (REF), defined as the closest N pixels from the island mask that do not belong to any IME region, where N is the number of pixels within the IME region excluding the shallow mask (Extended Fig. 1). When assessing the island impact on variables other than chlorophyll (i.e. primary production or PHYSAT), the region with the largest number of data pixels was adapted. Indeed, different datasets may have different data gaps, thus changing the number of data points in each region. To ensure that the number of data points remained identical in both regions, the region with most pixels was randomly subsampled to match the region with fewer pixels. The REF region was used to define the nearby Chl increase for each island (Chl_max relative to average Chl within REF). Detecting IMEs using a high sensitivity is justified on a climatological basis where spatial variability is heavily smoothed by a 17-year average; however, weak increases could result from noise. Statistics in Table 1 are thus presented both for all IMEs (more exhaustive) and after excluding IMEs with Chl increases near islands below 10% (more conservative).

PHYSAT. The PHYSAT method[37] is based on daily, 4-km resolution normalized water-leaving radiance (primary variable measured by a satellite ocean color radiometer after atmospheric correction, for several wavelengths). First, spectral radiance anomalies (Ra) are computed by removing a reference spectrum function of Chl for the same pixel, ensuring that the first order chlorophyll signal is removed. Then, these anomalies are clustered using an automatic unsupervised classification approach (self-organizing maps), classifying daily Ra into 100 "neuron groups" corresponding to a specific Ra spectral frequency shape and amplitude[56]. The number of neuron groups is reduced using phenological metrics to identify signals linked to specific phytoplankton assemblages[38], termed "phenoclasses" (61 for PHYSAT applied to

MODIS-Aqua). A previous version of PHYSAT was applied to the SeaWiFS satellite and matched with coincident *in situ* phytoplankton data, which enabled SeaWiFS phenoclasses to be labeled with six broad phytoplankton groups[57]. Phytoplankton labels are also available for MODIS phenoclasses, through SeaWiFS/MODIS matchups during their overlapping period. Around half of MODIS phenoclasses remain unlabeled, but could be matched to phytoplankton groups as more samples become available. The most common phenoclasses present in the tropical Pacific were labeled and found to be dominated by *Prochlorococcus*, *Synechococcus*, and nanoplankton. Daily MODIS phenoclasses (4 km resolution, July 2002 - April 2018) were averaged as a monthly climatology of phenoclass occurrence frequency at each pixel; pixels shallower than 30 m were removed. The corresponding product was used to calculate the phenoclass composition (percentage of occurrence for each phenoclass) within each IME and REF region detected previously. Ecological metrics were only computed in IME and REF regions including at least 100 PHYSAT data pixels, to ensure adequate PHYSAT coverage. This represents around half of the detected IMEs.

PHYSAT ecological metrics. Classical ecological metrics were computed from phenoclass proportions averaged in each IME and REF region, by regarding each phenoclass as a "species" in mathematical equations for each index. In practice, each phenoclass can contain varying numbers of species. However, phytoplankton richness is relatively stable in the tropics[11], so that the number of phytoplankton species belonging to each phenoclass should be relatively constant. Island impacts on phenoclass composition were assessed using the Bray-Curtis dissimilarity index[58] between each pair of IME and REF regions. The Bray-Curtis index can vary between 0 and 1, where 0 would indicate that IME and REF have the same phenoclass composition, and 1 that they do not share any phenoclasses. Island impacts on phenoclass diversity were assessed

570 using various biodiversity metrics: richness, Pielou's evenness[59], and the Shannon index[60]. These
571 metrics were computed in each IME and REF regions separately, and contrasted (similar to
572 chlorophyll and primary production). Just like true species richness strongly depends on
573 sampling effort, phenoclass richness increases with the number of pixels over which it is
574 computed (see Fig. S3). Phenoclass richness was corrected by rarefaction to 100 pixels to enable
575 direct statistical comparisons of richness across regions[61]. Computing biodiversity indices from
576 satellite products of phytoplankton taxonomy is not new. A previous study computed global
577 Shannon diversity metrics from PHYSAT six broad phytoplankton groups, identifying regional
578 hotspots matching known biodiversity hotspots[62]. While precise biodiversity estimates require an
579 extensive knowledge of the community, the De Monte index worked by capturing spatial
580 heterogeneity in dominant phytoplankton groups, which was shown to be highly correlated to
581 phytoplankton biodiversity in a model[63]. Here, by applying a similar method but using all 61
582 phenoclasses, we are exploiting the full power of the PHYSAT algorithm and capturing a more
583 precise picture of changes in phytoplankton taxonomy and biodiversity. This is a very powerful
584 approach because it bypasses the need to identify phytoplankton taxonomy from space. While
585 PHYSAT is only a proxy for phytoplankton taxonomy, broad phenoclass diversity patterns match
586 published phytoplankton biodiversity patterns such as increasing richness with phytoplankton
587 biomass in unproductive waters[43] (Extended Fig. 3).

Data availability statement

The main outputs of this study, including the island database, IME and REF masks, and IME impacts on chlorophyll, primary production, and PHYSAT, are available as a dataset hosted on Zenodo[64]. The PHYSAT climatology calculated for this paper is available there as well; PHYSAT is now being processed by ACRI (https://www.acri-st.fr/) and PHYSAT data will soon be publicly available from their website. Other data that support the findings of this study are available in various public repositories: https://coastwatch.pfeg.noaa.gov/erddap/info/index.html (MODIS chlorophyll concentration), http://science.oregonstate.edu/ocean.productivity/index.php (MODIS primary production), https://www.ngdc.noaa.gov/mgg/shorelines/gshhs.html (GSHHG coastline), https://www.gebco.net/data_and_products/gridded_bathymetry_data/ (GEBCO bathymetry). The Nunn et al. (2016) island database is available as an additional file accompanying their paper (https://doi.org/10.1186/s40562-016-0041-8).

Code availability statement

The IME detection algorithm, along with datasets and example code to reproduce Fig. 1, Extended Fig. 1, and parts of Table 1, is available at https://github.com/messiem/toolbox_IME_detection and the corresponding release published on Zenodo[65].

Additional references for the Methods section

51. Nunn, P. D., L. Kumar, I. Eliot & R. F. McLean (2016), Classifying Pacific islands, Geoscience Letters, 3(1), https://doi.org/10.1186/s40562-016-0041-8

52. Hasegawa, D., M. R. Lewis & A. Gangopadhyay (2009), How islands cause phytoplankton to bloom in their wakes, Geophys. Res. Lett., 36, L20605, https://doi.org/10.1029/2009GL039743

53. Platt, T. & S. Sathyendranath (1988), Oceanic Primary Production: Estimation by Remote Sensing at Local and Regional Scales, Science, 241(4873), 1613-1620, https://doi.org/10.1126/science.241.4873.1613

54. Hasegawa, D., H. Yamazaki, T. Ishimaru, H. Nagashima & Y. Koike (2008), Apparent phytoplankton bloom due to island mass effect, J. Mar. Sys., 69(3-4), 238-246, https://doi.org/10.1016/j.jmarsys.2006.04.019

55. Silsbe, G. M., M. J. Behrenfeld, K. H. Halsey, A. J. Milligan & T. K. Westberry (2016), The CAFE model: A net production model for global ocean phytoplankton, Glob. Biogeochem. Cycles, 30(12), 1756-1777, https://doi.org/10.1002/2016GB005521

56. Ben Mustapha, Z., S. Alvain, C. Jamet, H. Loisel & D. Dessailly (2014), Automatic classification of water-leaving radiance anomalies from global SeaWiFS imagery: Application to the detection of phytoplankton groups in open ocean waters, Remote Sens. Environ., 146, 97-112, https://doi.org/10.1016/j.rse.2013.08.046

57. Alvain, S., C. Moulin, Y. Dandonneau & H. Loisel (2008), Seasonal distribution and succession of dominant phytoplankton groups in the global ocean: A satellite view, Glob. Biogeochem. Cycles, 22(3), https://doi.org/10.1029/2007GB003154

58. Bray, J. R. & J. T. Curtis (1957), An Ordination of the Upland Forest Communities of Southern Wisconsin, Ecological Monographs, 27(4), 325-349, https://doi.org/10.2307/1942268

59. Pielou, E. (1966), The measurement of diversity in different types of biological collections, J. Theor. Biol., 13, 131-144, https://doi.org/10.1016/0022-5193(66)90013-0

60. Shannon, C. & W. Weaver (1948), Biodiversity measurements, The Mathematical Theory of Communication. Urbana University Press, Illinois, 117-27

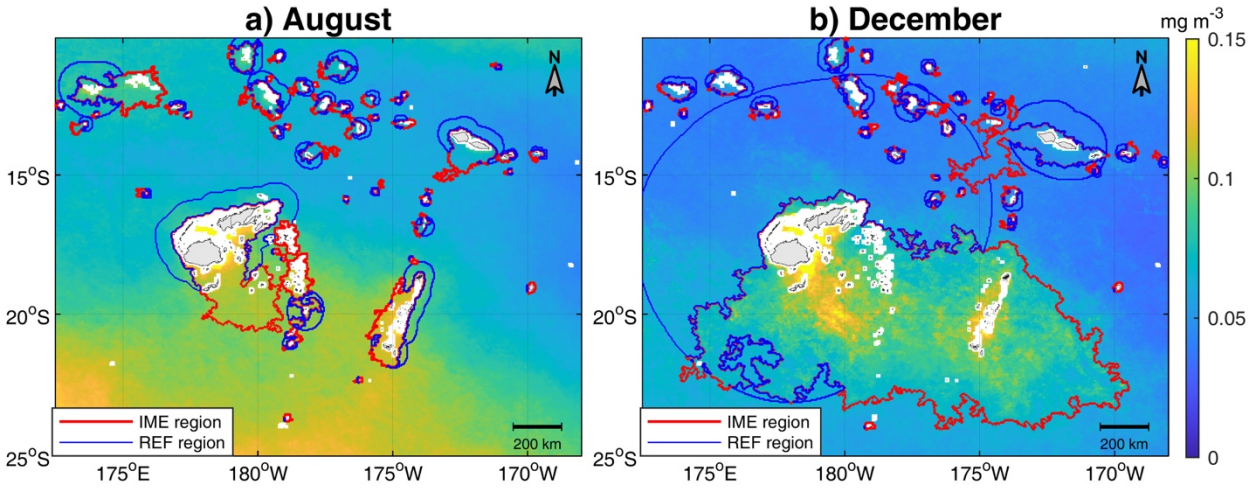
61. Colwell, R. K., C. X. Mao & J. Chang (2004), Interpolating, extrapolating, and comparing incidence-based species accumulation curves, Ecology, 85(10), 2717-2727, https://doi.org/10.1890/03-0557

62. De Monte, S., A. Soccodato, S. Alvain & F. d'Ovidio (2013), Can we detect oceanic biodiversity hotspots from space?, The ISME Journal, 7(10), 2054-2056, https://doi.org/10.1038/ismej.2013.72

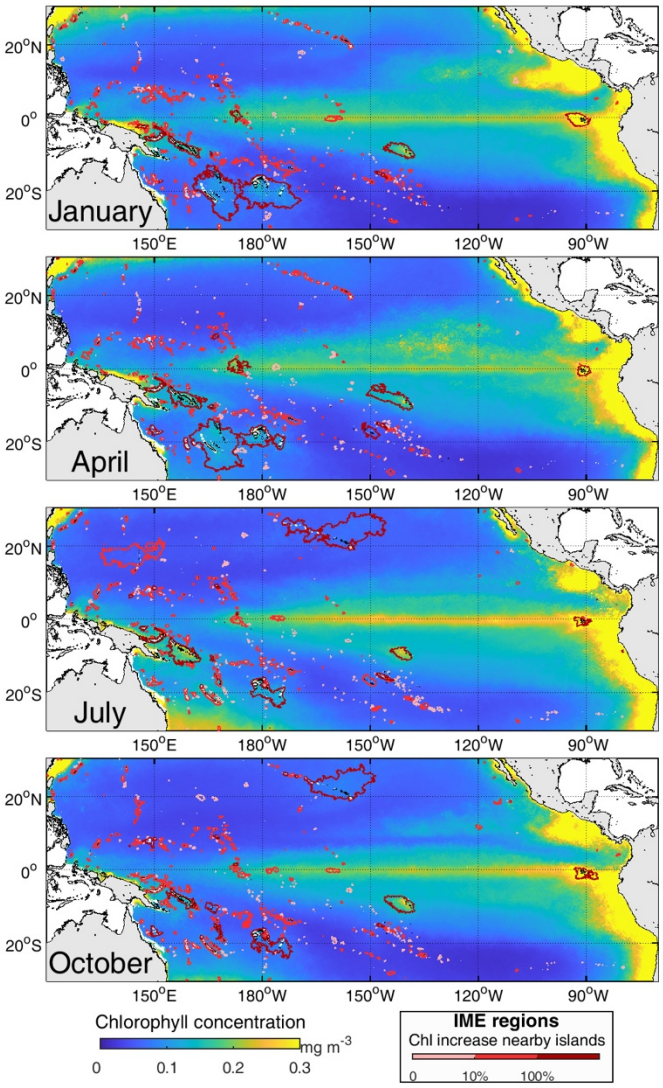
63. Soccodato, A., F. d'Ovidio , M. Lévy, O. Jahn, M. J. Follows & S. D. Monte (2016), Estimating planktonic diversity through spatial dominance patterns in a model ocean, Mar. Geonomics, 29, 9-17, https://doi.org/10.1016/j.margen.2016.04.015

64. Messié, M., A. Petrenko, A. Doglioli, E. Martinez & S. Alvain (2022), Data from: Basin-scale biogeochemical and ecological impacts of islands in the tropical Pacific Ocean (v1.0.0), Zenodo, https://doi.org/10.5281/zenodo.6416130

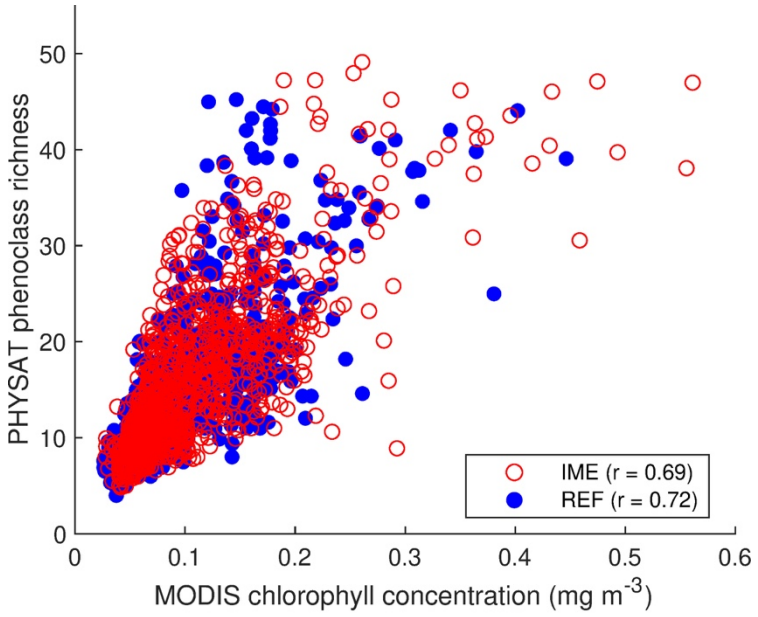
65. Messié, M. (2022), Code for: Basin-scale biogeochemical and ecological impacts of islands in the tropical Pacific Ocean (v1.0.0), Zenodo, https://doi.org/10.5281/zenodo.6494328



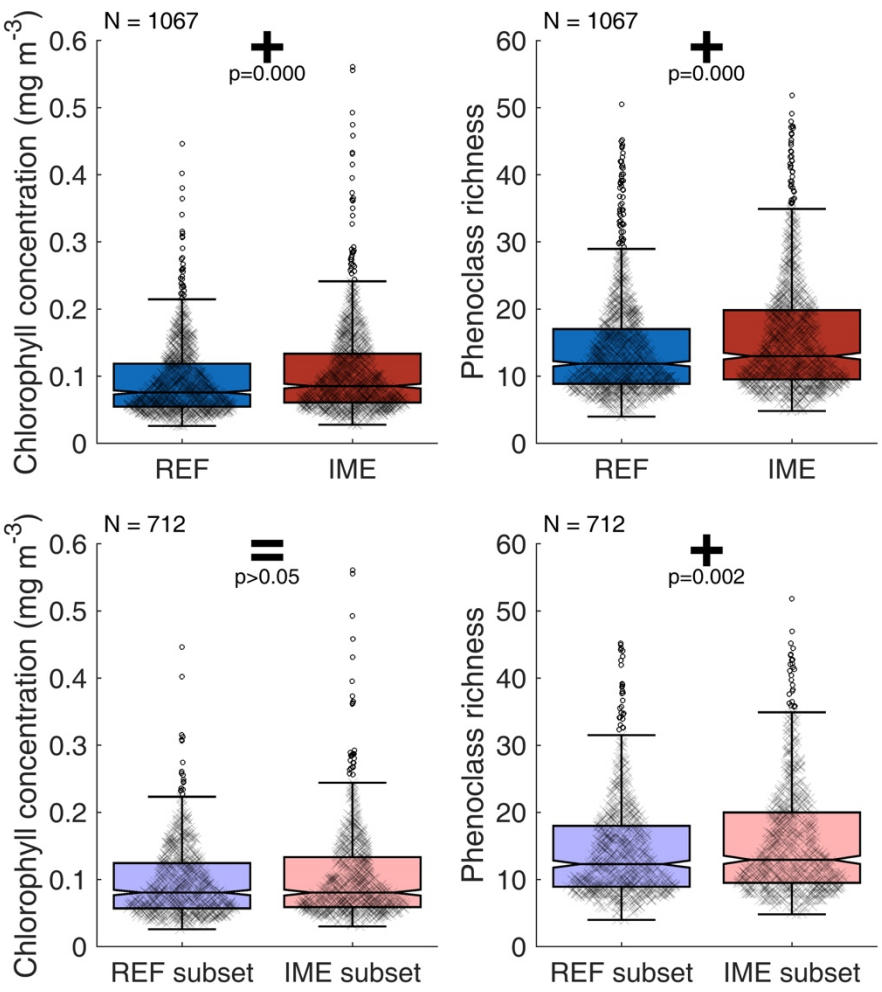
Extended Data Fig. 1: Example maps of IME and reference (REF) region detection. Two contrasting months are shown for the Fiji/Tonga region: a) August (small IMEs but higher climatological enrichment across the region), and b) December (strong IMEs, with IMEs from the Fiji and Tonga island groups merging). Reference regions (blue) exclude IME regions from any island.



Extended Data Fig. 2: IME maps for different climatological months. For each month, IME regions are contoured in different shades of red depending on Chl increase near islands relative to a reference region (similar to Fig. 1).



Extended Data Fig. 3: PHYSAT phenoclass richness vs Chl across IME and REF regions. Phenoclass richness was normalized to 100 data points, and only regions with at least 100 PHYSAT data points were included.



Extended Data Fig. 4: Example of random permutation used to remove the Chl signal on the phenoclass richness increase observed in IME regions. Top panel: identical to Fig. 3b left panels (that is, including all IME and REF regions); both Chl (left) and phenoclass richness (right) are significantly higher in IME than in REF regions (Mann-Whitney U-test). Bottom panel: example of a random permutation where 2/3 of the IME and REF regions were retained such that the Chl distributions do not significantly differ anymore. In this permutation, phenoclass richness remains significantly higher within the IME subset (right) even though Chl is (non-significantly) lower (left).

	All IMEs	IMEs with Chl increase nearby islands ≥ 10%
IME spatial impact		
IME area (in km²)	559 [172 – 2,051]	1,333 [430 – 3,965]
IME impact on Chl		
Nearby percentage Chl increase (in %)	11.4 [6.5 – 22.3]	19.9 [13.8 – 36.4]
Percentage Chl increase per IME (in %)	6.8 [4.4 – 10.8]	10.0 [7.3 – 14.2]
Total Chl increase per IME (in tons/m)	0.00 [0.00 – 0.01]	0.01 [0.00 – 0.04]
IME impact on primary production (PP)		
Percentage PP increase per IME (in %)	1.5 [0.3 – 3.5]	2.6 [0.9 – 5.3]
Total PP increase per IME (in TgC /yr)	0.00 [0.00 – 0.00]	0.00 [0.00 – 0.01]
IME impact on PHYSAT phenoclass diversity		
Percentage richness increase per IME (in %)	7.7 [-0.1 – 18.9]	8.9 [0.0 – 20.8]
Percentage evenness increase per IME (in %)	-0.3 [-6.4 – 6.0]	-0.3 [-6.6 – 6.2]
Percentage Shannon index increase per IME (in %)	2.9 [-1.7 – 8.7]	3.3 [-1.5 – 9.4]

Extended Data Table 1: Additional metrics for IME impacts in the tropical Pacific (see Table 1). Values are given as median [25th percentile – 75th percentile]. The extremely low values for total Chl and total primary production (intentionally kept in the same unit as in Table 1) highlight how a few major IMEs (visible in Fig. 1) are responsible for most of the large-scale impact on Chl and primary production.